Optical band structure and near-field intensity of a periodically arrayed monolayer of dielectric spheres on dielectric substrate of finite thickness

Y. Kurokawa* and H. Miyazaki
Department of Applied Physics, Tohoku University, Aramaki, Aoba, Sendai 980-8579, Japan

Y. Jimba
College of Engineering, Nihon University, Koriyama, Fukushima 963-8642, Japan
(Received 17 October 2003; published 30 April 2004)

We examined numerically the effect of the finite thickness substrate on the optical properties of a two-dimensional periodic dielectric sphere. The photonic band dispersion is obtained from the transmission spectra for general oblique incidence. These results are in good agreement with experimental ones. Transmission spectra and the band dispersion are found to be significantly modified from those without substrate. This change is well explained by the anticrossing of eigenstates of the monolayer spheres and those bounded within the substrate. The characteristic feature of near-field intensity is investigated in detail when the eigenstates of the system are excited by the incident light. It is shown that the near-field intensity gives important information to figure out the origin of eigenstates. In addition, the shape of intensity distribution is analyzed by using the amplitudes of diffracted lights.

DOI: 10.1103/PhysRevB.69.155117 PACS number(s): 42.70.Qs, 42.25.Bs, 42.79.−e

I. INTRODUCTION

Recently, there has been growing interest in the control of light propagation by using photonic crystals (PhC's).[1] PhC's are artificial photonic materials which can freely navigate electromagnetic waves. They are characterized by the periodicity of the dielectric constant comparable with the wavelength of light. This periodicity brings about the photonic band structure accompanied with photonic band gaps (PBG's). Propagation of the light within PBG's is forbidden in PhC's. At the early stage of researches, PhC's with PBG's in all directions (complete PBG's) attracted much interest,[2] because there was a strong demand to control the spontaneous emission of atomic systems. Recently, there also arose special interest in the application of band dispersion relations in PhC's since the discovery of superprism and superlens effects.[3] To realize these effects, it is essential to fabricate PhC's of extremely high quality. Very sophisticated technology is required to create such three-dimensional PhC's. In contrast, two-dimensional PhC's are relatively easy to fabricate. Various slab-type two-dimensional PhC's are developed.[4] One of such slab-type PhC is a two-dimensional periodic dielectric sphere on a dielectric substrate.

A monolayer of periodic dielectric spheres is an important system for the physical understanding of the origin of photonic band structures. In PhC's, periodic arrangement of dielectric objects play the same role of potential with that of periodic atoms for electrons in semiconductors. Electrons in semiconductors are tightly bound to each atom and can hop from atom to atom to form the band structure. The same phenomenon occurs in PhC's. In the case of dielectric spheres, a bound state of each sphere corresponds to the Mie resonance state. When spheres are arrayed periodically, photons can hop from one sphere to its neighbor. This hopping process gives rise to photonic band structures. Photonic band structures of monolayer dielectric spheres without substrate have been calculated by the vector Korringa-Kohn-Rostoker (KKR) method[5,6] with very high accuracy and fast convergence.[7–10]

A variety of experimental reports can be found on the two-dimensional periodic dielectric spheres created, for example, by the self-assembly method[11,12] or the micromanipulation technique.[13] Good agreement is obtained between theory and experiment on Si_3N_4 sample in the millimeter wavelength region.[14] This agreement is due to very good sample quality. In addition, they use very thin substrate which can effectively be ignored. On the other hand, typical crystals in visible or infrared region are made of polystyrene or polyvinyltoluene spheres on the substrate of semi-infinite[11,12] or finite thickness.[13] At present, we cannot yet obtain such good quantitative agreement between theory and experiment as those found for samples without substrate.

In the system of the two-dimensional periodic dielectric spheres, electromagnetic energy can dissipate into the vacuum through a direction perpendicular to the sample layer. In the present work, we focus on the wavelength range comparable with the size of a sphere, that is, we deal with the Mie resonance[15,16] region of $\ell \leqslant 5$. Hence, light can hardly localize within spheres and leaks outside. This leakage of light from spheres induces interaction with surrounding objects. Therefore, light interacts not only with surrounding spheres but also with the substrate. Interaction with the substrate is expected to change significantly the optical properties of the system. So far, there have been a few theoretical papers which have dealt with the two-dimensional periodic spheres on a substrate.[17–20] To the authors' knowledge, however, no theoretical work has been presented which discusses the effect of the substrate from the point of view of photonic band structures.

In a recent paper, we have briefly reported numerical results of transmission spectra for perpendicular incidence from a monolayer dielectric spheres on a substrate.[21] We found that dips of transmission spectra become much broad without significantly changing their positions in the case of

the semi-infinite substrate. This broadening is caused by the dissipation of electromagnetic energy into the semi-infinite substrate. When the substrate is finite, on the other hand, we observed significant change of transmission spectra. This change is brought about by the presence of eigenstates within the substrate which interacts with those of spheres.

In this paper, we report the results of detailed investigation on the general optical properties of a two-dimensional periodic dielectric spheres on a substrate of finite thickness. We present the band dispersion relation obtained from transmission spectra for general oblique incidence. We also report the characteristic feature of the distribution of electric field intensity near the sample surface (near-field intensity) when eigenstates of the system are excited by the incident light. It is shown that these near-field intensity can bring about important information concerning the origin of the drastic change of the spectrum. The near-field intensity can be observed by recently developed scanning near-field optical microscope (SNOM).[11,22,23]

This paper is organized as follows. Our model and theoretical framework are described in Sec. II. Results and discussions for perpendicular incidence are discussed in Sec. III. We first deal with transmission spectra and discuss their dependence on thickness of the substrate. Next, we investigate the origin of eigenstates of the system from the point of view of near-field intensity. Section IV deals with results and discussions for oblique incidence. From transmission spectra for general oblique incidence, we draw band dispersions for *s* and *p* polarization. We also give a detailed discussion of the change of near-field intensity at the cross point of two band branches. Section V is devoted to summary.

II. MODEL AND FORMULATION

We deal with a monolayer of two-dimensional periodic dielectric spheres on a substrate of finite thickness as shown in Fig. 1. Radius and dielectric constant of spheres are denoted by a and ϵ_Q, respectively. Spheres are in contact with each other and are arranged within the xy plane to form a triangular lattice. The dielectric constant and thickness of the substrate are ϵ_S and d, while the dielectric constant of vacuum is denoted by ϵ_0. The origin of coordinates is chosen at the center of one of the spheres. Plane electromagnetic wave of wave vector $\mathbf{k}_0=(\mathbf{k}_{//},\Gamma_0^+)$ and amplitude E_i^0 is incident upward from below the substrate;

$$E_i(\mathbf{r})=E_i^0\exp(i\mathbf{k}_0\cdot\mathbf{r}), \tag{1}$$

where $i=x,y$, or z, and $\mathbf{k}_{//}=(k_x,k_y)$ is the in-plane component of $\mathbf{k}_0$. Γ_0^+ is the z component of $\mathbf{k}_0$ and is given from the energy-conservation law as $+\sqrt{\mathbf{k}_0^2-\mathbf{k}_{//}^2}$. The polarization of incident light is also indicated in Fig. 1(a).

Let us briefly describe the scattering process of the present system. The incident light from the substrate is multiply scattered within the monolayer of spheres. The scattered light acquires two-dimensional reciprocal lattice vectors $\mathbf{h}$ by the umklapp process due to periodicity of the monolayer. Thus, the wave vector of the scattered light is given as $\mathbf{k}_\mathbf{h}^\pm=(\mathbf{k}_{//}+\mathbf{h},\Gamma_\mathbf{h}^\pm)$, where $\Gamma_\mathbf{h}^\pm=\pm\sqrt{\mathbf{k}_0^2-(\mathbf{k}_{//}+\mathbf{h})^2}$.

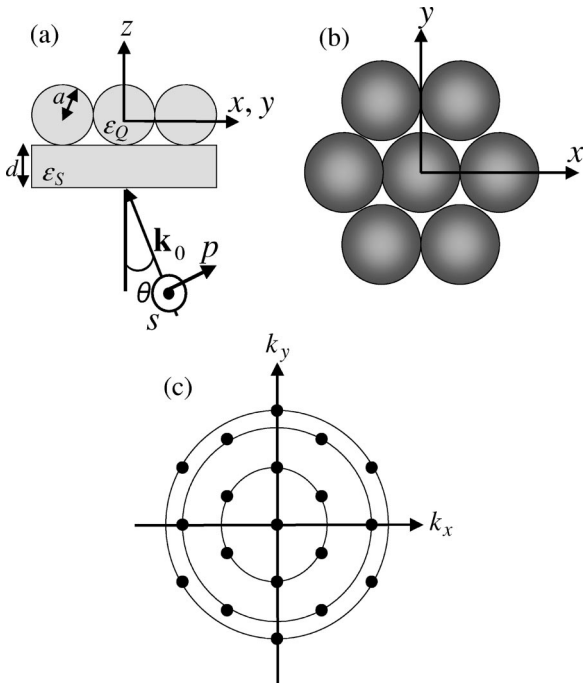

FIG. 1. (a) Two-dimensional periodic dielectric spheres of radius a and dielectric constant ϵ_Q on a substrate of finite thickness d and dielectric constant ϵ_S. Spheres are in contact with each other within the xy plane and form a triangular lattice. Plane electromagnetic wave of wave vector $\mathbf{k}_0=(\mathbf{k}_{//},\Gamma_0^+)$ and s or p polarization is incident upward from below the substrate with incident angle θ. (b) Real and (c) reciprocal spaces of the triangular lattice. Reciprocal-lattice vectors of the same length belong to the same shell. The origin of the reciprocal lattice is taken as the 0th shell. Shells of first, second, and third nearest neighbors from the origin are called as the first, second, and third shell, respectively.

Note that the scattered light is either propagating or evanescent wave if $\Gamma_\mathbf{h}^\pm$ is real or imaginary, respectively. Part of the scattered light is incident on the substrate, scattered multiply within the substrate and reflected back again onto the monolayer.

The multiple scattering process within the monolayer has already been presented by the matrix formulation.[5,6,22] We will simply summarize the results as follows. We expand the plane incident wave in terms of vector spherical harmonics and take into account the multiple scattering within the monolayer rigorously by using the Green's function. Vector spherical waves emerging from the monolayer after multiple scattering are then expanded in terms of plane waves. Thus, transmitted and reflected lights from the monolayer are related with amplitudes $E_{j,\mathbf{h}'}$ of incident plane waves as follows:

$$E_{i,\mathbf{h}}^{\pm\pm}(Q)=\sum_{j,\mathbf{h}'}U_Q^{\pm\pm}(i,\mathbf{h};j,\mathbf{h}')E_{j,\mathbf{h}'}, \tag{2}$$

where superscripts indicate the propagation direction of each wave along the z axis. In Eq. (2), we assume general wave vector $\mathbf{k}_\mathbf{h}^\pm=(\mathbf{k}_{//}+\mathbf{h},\Gamma_\mathbf{h}^\pm)$ for incident waves in order to deal with reflected propagating and evanescent waves from the

substrate. In the numerical calculation, we take into account $\ell_{max}=9$ for the expansion in terms of spherical harmonics.

Let us next treat the multiple reflection process within the substrate. To describe the scattering process concerning the substrate, we introduce 3×3 interface matrices which relate transmitted and reflected waves on the surface of the substrate. The wave vector of the incident light onto the substrate from above is given by $\mathbf{k}_{\mathbf{h}}^{-}=(\mathbf{k}_{//}+\mathbf{h},\Gamma_{\mathbf{h}}^{-})$. From the energy conservation law, the z component of the wave vector inside and outside the substrate are given as $\gamma_0(\mathbf{h})=\sqrt{\epsilon_0\mathbf{k}_0^2-(\mathbf{k}_{//}+\mathbf{h})^2}$ and $\gamma_S(\mathbf{h})=\sqrt{\epsilon_S\mathbf{k}_0^2-(\mathbf{k}_{//}+\mathbf{h})^2}$, respectively. Note that $\gamma_0(\mathbf{h})$ and $\gamma_S(\mathbf{h})$ are taken to be either positive real or positive imaginary. It is straightforward to show from the boundary condition at the surface that interface matrices of the upper surface of the substrate is given by

$$T^{--}(\mathbf{h};\epsilon_0,\epsilon_S)=\begin{pmatrix} \frac{2\gamma_0(\mathbf{h})}{\gamma_0(\mathbf{h})+\gamma_S(\mathbf{h})} & 0 & \frac{-2\gamma_0(\mathbf{h})(\epsilon_0-\epsilon_S)(\mathbf{k}_{//}+\mathbf{h})_x}{[\gamma_0(\mathbf{h})\epsilon_S+\gamma_S(\mathbf{h})\epsilon_0][\gamma_0(\mathbf{h})+\gamma_S(\mathbf{h})]} \\ 0 & \frac{2\gamma_0(\mathbf{h})}{\gamma_0(\mathbf{h})+\gamma_S(\mathbf{h})} & \frac{2\gamma_0(\mathbf{h})(\epsilon_0-\epsilon_S)(\mathbf{k}_{//}+\mathbf{h})_y}{[\gamma_0(\mathbf{h})\epsilon_S+\gamma_S(\mathbf{h})\epsilon_0][\gamma_0(\mathbf{h})+\gamma_S(\mathbf{h})]} \\ 0 & 0 & \frac{-2\gamma_0(\mathbf{h})\epsilon_0}{\gamma_0(\mathbf{h})\epsilon_S+\gamma_S(\mathbf{h})\epsilon_0} \end{pmatrix}, \tag{3}$$

$$R^{+-}(\mathbf{h};\epsilon_0,\epsilon_S)=\begin{pmatrix} \frac{\gamma_0(\mathbf{h})-\gamma_S(\mathbf{h})}{\gamma_0(\mathbf{h})+\gamma_S(\mathbf{h})} & 0 & \frac{-2\gamma_0(\mathbf{h})(\epsilon_0-\epsilon_S)(\mathbf{k}_{//}+\mathbf{h})_x}{[\gamma_0(\mathbf{h})\epsilon_S+\gamma_S(\mathbf{h})\epsilon_0][\gamma_0(\mathbf{h})+\gamma_S(\mathbf{h})]} \\ 0 & \frac{\gamma_0(\mathbf{h})-\gamma_S(\mathbf{h})}{\gamma_0(\mathbf{h})+\gamma_S(\mathbf{h})} & \frac{-2\gamma_0(\mathbf{h})(\epsilon_0-\epsilon_S)(\mathbf{k}_{//}+\mathbf{h})_y}{[\gamma_0(\mathbf{h})\epsilon_S+\gamma_S(\mathbf{h})\epsilon_0][\gamma_0(\mathbf{h})+\gamma_S(\mathbf{h})]} \\ 0 & 0 & \frac{\gamma_0(\mathbf{h})\epsilon_S-\gamma_S(\mathbf{h})\epsilon_0}{\gamma_0(\mathbf{h})\epsilon_S+\gamma_S(\mathbf{h})\epsilon_0} \end{pmatrix} \tag{4}$$

for the incident light from the upper side. Interface matrices of the upper surface for the light incidence from below are obtained from Eqs. (3) and (4) by interchanging ϵ_0 and $\gamma_0(\mathbf{h})$ with ϵ_S and $-\gamma_S(\mathbf{h})$, respectively. They are denoted as $T_{i,j}^{++}(\mathbf{h};\epsilon_0,\epsilon_S)$ and $R_{i,j}^{-+}(\mathbf{h};\epsilon_0,\epsilon_S)$. For the substrate of finite thickness, we also need interface matrices of lower surface. They can be obtained similarly and are denoted as $T_{i,j}^{++}(\mathbf{h};\epsilon_S,\epsilon_0)$, $R_{i,j}^{-+}(\mathbf{h};\epsilon_S,\epsilon_0)$, $T_{i,j}^{--}(\mathbf{h};\epsilon_S,\epsilon_0)$, and $R_{i,j}^{+-}(\mathbf{h};\epsilon_S,\epsilon_0)$. Finally, we introduce propagation matrices within the substrate as

$$P_{i,j}^{\pm}(\mathbf{h};\epsilon_S)=\exp\{\pm i\gamma_S(\mathbf{h})d\}\delta_{i,j}. \tag{5}$$

To describe the multiple reflection of the light incident from the upper side of the substrate, it is convenient to use the following 3×3 matrix:

$$Q^{-}(\mathbf{h};\epsilon_0,\epsilon_S)=[\delta_{ij}-R^{-+}(\mathbf{h};\epsilon_0,\epsilon_S)P^{+}(\mathbf{h};\epsilon_S)\times R^{+-}(\mathbf{h};\epsilon_S,\epsilon_0)P^{-}(\mathbf{h};\epsilon_S)]^{-1}. \tag{6}$$

Then, transmitted and reflected lights, $E_i^{--}(S)$ and $E_i^{+-}(S)$, are given in terms of $Q^{-}(\mathbf{h};\epsilon_0,\epsilon_S)$ as

$$E_{i,\mathbf{h}}^{--}(S)=\sum_{j,j_1,j_2,j_3} T_{i,j_1}^{--}(\mathbf{h};\epsilon_S,\epsilon_0)P_{j_1,j_2}^{-}(\mathbf{h};\epsilon_S)\times Q_{j_2,j_3}^{-}(\mathbf{h};\epsilon_0,\epsilon_S)T_{j_3,j}^{--}(\mathbf{h};\epsilon_0,\epsilon_S)E_{j,\mathbf{h}} \equiv\sum_j U_S^{--}(i,j;\mathbf{h})E_{j,\mathbf{h}}, \tag{7}$$

$$E_{i,\mathbf{h}}^{+-}(S)=\sum_j\Bigg[R_{i,j}^{+-}(\mathbf{h};\epsilon_0,\epsilon_S)+\sum_{j_1,j_2,j_3,j_4,j_5} T_{i,j_1}^{++}(\mathbf{h};\epsilon_0,\epsilon_S)P_{j_1,j_2}^{+}(\mathbf{h};\epsilon_S)\times R_{j_2,j_3}^{+-}(\mathbf{h};\epsilon_S,\epsilon_0)P_{j_3,j_4}^{-}(\mathbf{h};\epsilon_S)\times Q_{j_4,j_5}^{-}(\mathbf{h};\epsilon_0,\epsilon_S)T_{j_5,j}^{--}(\mathbf{h};\epsilon_0,\epsilon_S)\Bigg]E_{j,\mathbf{h}} \equiv\sum_j U_S^{+-}(i,j;\mathbf{h})E_{j,\mathbf{h}}. \tag{8}$$

The case of the light incidence from the lower side of the substrate can be treated similarly.

The multiple reflection between the monolayer and the substrate is taken into account by the bilayer method. It is easy to show that transmitted and reflected lights, E_i^{++} and E_i^{-+}, for incidence from below the system are respectively given as

$$E_{i,\mathbf{h}}^{++}=\sum_{j,j_1,j_2,\mathbf{h}'} U_Q^{++}(i,\mathbf{h},j_1,\mathbf{h}')W^{+}(j_1,\mathbf{h}';j_2,\mathbf{h}=\mathbf{0})\times U_S^{++}(j_2,j;\mathbf{h}=\mathbf{0})E_{j,\mathbf{0}} \equiv\sum_j U^{++}(i,\mathbf{h},j,\mathbf{h}=\mathbf{0})E_{j,\mathbf{0}}, \tag{9}$$

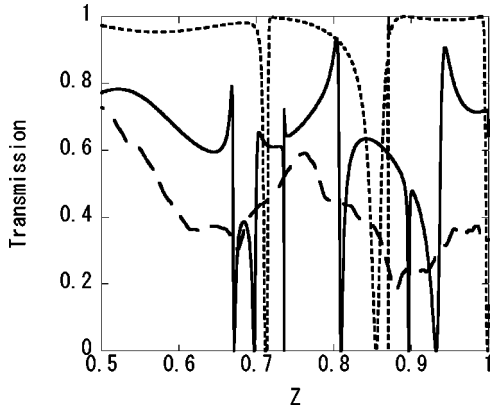

FIG. 2. Transmission spectra for perpendicular incidence. Here, $\epsilon_Q=2.56$, $a=1.0$ μm, $\epsilon_S=4.41$, and $d=0.3$ μm. The vertical and horizontal axes are transmission and normalized frequency $Z=\sqrt{3}a/\lambda$, respectively. Solid and dotted lines represent, respectively, theoretical results with and without substrate (Ref. 22), and the broken line is the experimental result (Ref. 13).

$$E^{-+}_{i,\mathbf{h}}=\sum_{j,\mathbf{h}'}\Big[U_S^{-+}(i,j;\mathbf{h}=\mathbf{0}) + \sum_{j_1,j_2,j_3} U_S^{--}(i,j_1;\mathbf{h})U_Q^{-+}(j_1,\mathbf{h};j_2,\mathbf{h}') \times W^{+}(j_2,\mathbf{h}';j_3,\mathbf{h}=\mathbf{0})U_S^{++}(j_3,j;\mathbf{h}=\mathbf{0})\Big]E_{j,\mathbf{0}}$$

$$\equiv\sum_j U^{-+}(i,\mathbf{h};j,\mathbf{h}=\mathbf{0})E_{j,\mathbf{0}}. \tag{10}$$

Here, the matrix $W^{+}(i,\mathbf{h}';j,\mathbf{h})$ describes the multiple reflection between the monolayer and the substrate and is given by

$$W^{+}=[I-U_S^{-+}(\mathbf{h}')U_Q^{+-}(\mathbf{h}';\mathbf{h})]^{-1}, \tag{11}$$

where $I_{i,\mathbf{h}';j,\mathbf{h}}=\delta_{i,j}\delta_{\mathbf{h},\mathbf{h}'}$. The case of the light incidence from the upper side of the system can be treated similarly.

The transmission T of the system is calculated from the electromagnetic energy flow towards the incidence direction,

$$T=\sum_i\left|\sum_j U^{++}(i,\mathbf{k}_0;j,\mathbf{k}_0)E_{j,\mathbf{0}}\right|^2, \tag{12}$$

for unit amplitude of the incident light with wavelength λ. In the numerical calculation, the velocity of light c in the vacuum is taken as $c=1$, and frequency and wave number are measured in units of dimensionless parameter $Z=\sqrt{3}a/\lambda$. In this paper, the calculation was carried out in the range of $Z\leqslant 1.0$, and 19 reciprocal-lattice vectors within the third shell in Fig. 1(c) were taken into account.

III. RESULTS AND DISCUSSIONS FOR PERPENDICULAR INCIDENCE

Figure 2 shows the transmission spectra for perpendicular incidence. Dielectric constant and radius of spheres are 2.56 and 1.0 μm, while dielectric constant and thickness of the substrate are 4.41 and 0.3 μm, respectively. Solid and dotted lines represent theoretical results with and without the substrate,[22] respectively, and the broken line is the experimental result.[13] The calculated transmission spectrum in the presence of the substrate shows six dips at $Z=0.671$, 0.698, 0.736, 0.808, 0.896, and 0.936, while that without the substrate has only three dips at $Z=0.712$, 0.855, and 0.870. Thus, the presence of the substrate significantly changes the spectrum. The experimental result, on the other hand, shows only two broad dips at $Z=0.68$ and 0.88. While the theoretical result approaches the experimental one, agreement is not so good as in the case of the semi-infinite substrate.[21] This difference seems to be attributed to the presence of disorder in the arrangement of spheres in the experiment. In addition, total number of spheres is limited to 91 in the experiment. If these effects cause smearing of sharp dips in the spectrum, the theoretical result agrees comparatively well with the experimental one.

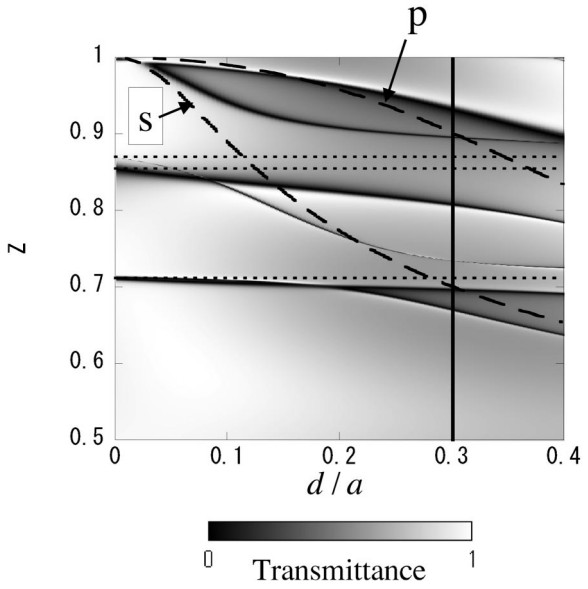

FIG. 3. Transmission spectra for perpendicular incidence in the range of $0\leqslant d/a\leqslant 0.4$ and fixed value of $\epsilon_S=4.41$. The horizontal and the vertical axes are thickness of the substrate d/a and normalized frequency Z, respectively. The darker region corresponds to the lower transmission. The vertical solid line at $d/a=0.3$ corresponds to the transmission spectrum of Fig. 2. Horizontal dotted lines at $Z=0.712$, 0.855, and 0.870 represent the eigenfrequencies of the monolayer spheres, while lower and upper broken lines in the figure correspond to *s*- and *p*-polarized eigenstates of the substrate, respectively.

In order to clarify the origin of dips in Fig. 2, we examine the dependence of transmission spectra on thickness of the substrate. Figure 3 shows the transmission spectrum in the range of $0\leqslant d/a\leqslant 0.4$ for fixed value of $\epsilon_S=4.41$. The darker region corresponds to the lower transmission. In contrast to the case of the semi-infinite substrate, dips do not broaden significantly. The vertical solid line at $d/a=0.3$ corresponds to the transmission spectrum of Fig. 2. Horizontal dotted lines at $Z=0.712$, 0.855, and 0.870 represent the eigenfrequencies of the monolayer as shown by the dips of dotted line in Fig. 2. Detailed calculation shows that eigen-

states at $Z=0.712$ are almost doubly degenerate. Broken lines show the eigenstates of the substrate. They are obtained from the condition that diffracted lights with reciprocal-lattice vectors of the first shell are in resonance within the substrate, i.e., $\det[Q^{-}(i,j;\mathbf{h})]=0$. We therefore have

$$\exp\{i\gamma_S(\mathbf{h})d\}\left(\frac{\gamma_0(\mathbf{h})-\gamma_S(\mathbf{h})}{\gamma_0(\mathbf{h})+\gamma_S(\mathbf{h})}\right)=1, \tag{13}$$

$$\exp\{i\gamma_S(\mathbf{h})d\}\left(\frac{\gamma_S(\mathbf{h})\epsilon_0-\gamma_0(\mathbf{h})\epsilon_S}{\gamma_0(\mathbf{h})\epsilon_S+\gamma_S(\mathbf{h})\epsilon_0}\right)=1, \tag{14}$$

where Eqs. (13) and (14), respectively, correspond to the *s* and *p* polarization. They are plotted by lower and upper broken lines in Fig. 3. These resonance states appear in the range of $|\mathbf{h}|/\epsilon_S \leqslant Z \leqslant |\mathbf{h}|$ in which the diffracted light within the substrate is totally reflected at the interface of the substrate.

From Fig. 3, we can interpret the transmission spectrum of the system as a crossover phenomenon between eigenstates of the substrate and those of the monolayer. Degeneracy of eigenstates at $Z=0.712$ is lifted by the interaction with those of *s* polarization near $d/a=0.3$. This is also the case for the eigenstate of the monolayer at $Z=0.870$ which appears as a sharp dip in the spectrum. On the other hand, the eigenstate of the monolayer at $Z=0.855$ appearing as a broad dip in the spectrum does not interact with that of the substrate of *s*-polarization, because the solid line clearly crosses the broken line of *s* polarization. Instead, this eigenstate interacts with that of the substrate of *p* polarization. This difference of interaction originates from the distribution of electric field and will be clarified by the near-field intensity below.

In the previous work, we have examined the dependence of transmission spectra on dielectric constants of the substrate by fixing thickness of substrate.[21] From the result, we show that the optical property of the system can be controlled by changing the dielectric constant of the substrate. However, dielectric constant of the substrate can only be varied for a limited range. In contrast, thickness of the substrate is changeable in a wide range. Therefore, it would be much better to adjust thickness instead of dielectric constant in order to design the optical property of the system.

Dips in transmission spectra represent the excitation of eigenstates of the system. In the present system, the eigenstates of the whole system are approximately given by the linear combination of those of the monolayer and the substrate. When eigenstates are excited, there occurs the enhancement of near field due to large evanescent components of diffracted lights. As a result, the electric field is localized near the system.[22,23] Consequently, the near-field intensities are best suited for distinguishing the difference of excitation between these eigenstates.

Near-field intensities are obtained from amplitudes of the electric field $E_i(\mathbf{h})$ by the following equation:

$$E_i(\mathbf{r})=\sum_{\mathbf{h}} E_i(\mathbf{h})\exp\{i\mathbf{k}_{\mathbf{h}}^{\pm}\cdot(\mathbf{r}-\mathbf{r}_0^{\pm})\}, \tag{15}$$

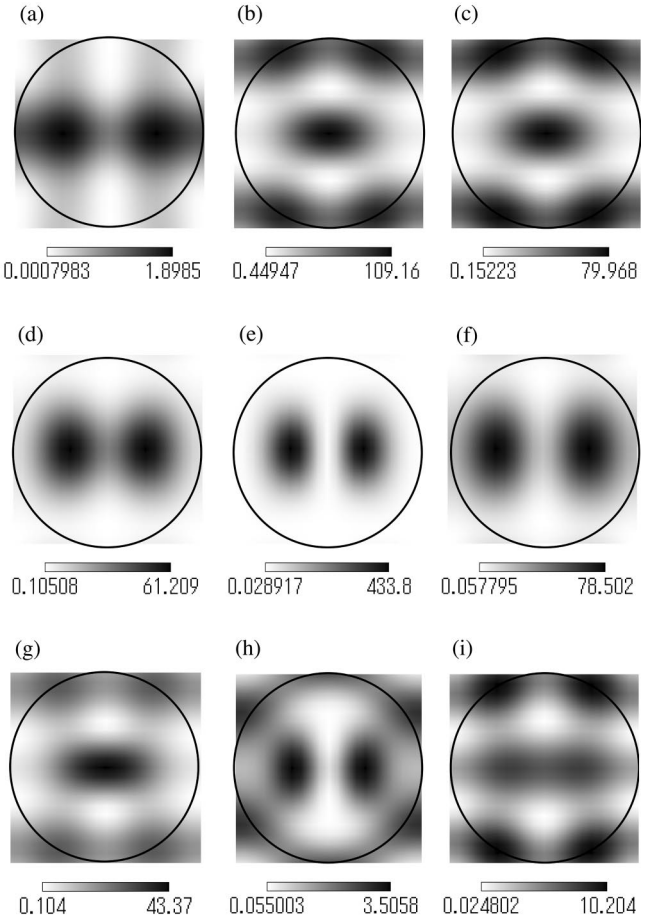

FIG. 4. Near-field intensity at dips of $Z=0.671$ in (a–c), $Z=0.808$ in (d–f), and $Z=0.896$ in (g–i) in Fig. 2. The incident light is chosen to be *x* polarization. The electric-field intensity is plotted just above the spheres in (a), (d), and (g), on the upper plane of substrate in (b), (e), and (h) and on the lower plane of substrate in (c), (f), and (i). The darker region corresponds to larger electric-field intensity.

where $\mathbf{r}_0^{\pm}=(0,0,\pm a)$. Superscripts $\pm$ of $\mathbf{k}_{\mathbf{h}}$ and $\mathbf{r}_0$ correspond to a near field above and below the spheres, respectively. The near-field intensity can be observed by the SNOM.[11] Figure 4 shows the near-field intensity at dips of $Z=0.671$, 0.808, and 0.896 in Fig. 2. Incident light is chosen to be *x*-polarized. The electric-field intensity is plotted just above the spheres in Figs. 4(a), 4(d), and 4(g), on the upper plane of the substrate in Figs. 4(b), 4(e), and 4(h), and on the lower plane of the substrate in Figs. 4(c), 4(f), and 4(i). The darker region corresponds to larger field intensity.

Figures 4(a), 4(b), and 4(c) show near-field intensity at $Z=0.671$. One can see two small black circles on the *x* axis in Fig. 4(a). These circles are due mainly to the *x* component of the electric field. On the other hand, we observe large electric field both at the center of spheres and at contact points with adjacent spheres in Figs. 4(b) and 4(c). Besides, we observe huge enhancement of electric field in Figs. 4(b) and 4(c). From these facts, we conclude that dip at $Z=0.671$ represents the eigenstate of the substrate. Figures 4(d), 4(e), and 4(f) show near-field intensity at $Z=0.808$. We observe significant enhancement of the electric field in Fig.

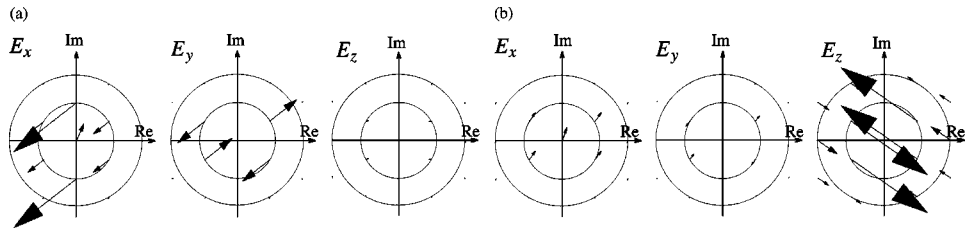

FIG. 5. Vector representation of $E_i(\mathbf{h})$. Real and imaginary part of each $E_i(\mathbf{h})$, respectively, correspond to horizontal and vertical components, and origin is taken at each **h**. (a) and (b) correspond to Figs. 4(b) and 4(e), respectively.

4(e) on the upper plane of substrate which is about 433 times larger than the incident light. This enhancement is the largest of all cases for perpendicular incidence. We also note that electric field is much enhanced on the monolayer compared to the case of Fig. 4(a). Therefore, the electric-field distribution is relatively extended within the system, covering both the monolayer and the substrate. This dip turns out to be the mixed state of the monolayer and the substrate. Figures 4(g), 4(h), and 4(i) show near-field intensity at $Z=0.896$. Electric field is the largest above the monolayer. Thus, this dip is identified as the eigenstate of the monolayer spheres.

Near-field intensity at $Z=0.671$ and 0.808 are enhanced near the substrate. However, the shape of intensity distribution is different. We study the origin of this difference from the amplitude of diffracted lights. Figure 5 shows the vector representation of $E_i(\mathbf{h})$, where real and imaginary parts of each $E_i(\mathbf{h})$ correspond to horizontal and vertical component, respectively. The origin is taken at each **h**. Figures 5(a) and 5(b) correspond to Figs. 4(b) and 4(e), respectively. We found that the magnitude of $E_i(\mathbf{h})$ belonging to the first shell is ten times larger than those of the second shell in Figs. 5(a) and 5(b). Therefore, near-field intensities are mainly composed of the zeroth and the first shell components. It is easy to show from Eq. (15) that the ellipse at the center of Fig. 4(b) is due to the large x component in Fig. 5(a), while enhancement of the electric field at the contact points of spheres in Fig. 4(b) is ascribed to the y component. On the other hand, the z component can be ignored in Fig. 5(a). Note that the eigenstates of the substrate of s-polarization have only the in-plane component too. Therefore, the dip at $Z=0.671$ arise from the excitation of s polarized eigenstate of the substrate. In contrast, larger z component in Fig. 5(b) produces two ellipses on the x axis in Fig. 4(e). We should note that eigenstates of the substrate of p polarization has large z component. Accordingly, this dip arises from the p-polarized eigenstate of the substrate.

IV. RESULTS AND DISCUSSIONS FOR OBLIQUE INCIDENCE

In this section, we discuss numerical results for oblique incidence. The present system exhibits the two-dimensional photonic band dispersion due to the periodicity. The band structure can be obtained from transmission spectra for oblique incidence[13,22,24] in the following way. Dips in transmission spectra reflect the excitation of eigenstates of the system. Due to the translation symmetry within the x-y plane, the excited eigenstate has the same in-plane wave vector $k_{//}=Z\sin\theta$ with that of incident light. In-plane wave vector $k_{//}=Z\sin\theta$ can be scanned by changing incident angle θ. Accordingly, the dispersion relation can be obtained by changing θ and tracing the dips of transmission spectra. Note that the excitation of the eigenstate depends on the polarization of incident light. Therefore, we calculate the dispersion relation of both polarizations.

Let us show a series of transmission spectra of p polarization in Fig. 6(b) for ΓK direction and Fig. 6(c) for ΓM direction. Incidence angles are chosen as 10°, 20°, 30°, and 40°. Solid and dotted lines are theoretical and experimental results,[13] respectively. Theoretical results show that degenerate states for perpendicular incidence split into a set of very complicated states as θ is increased. While a direct correspondence between experimental and theoretical results is difficult, overall feature seems to be in agreement if theoretical results are smeared out because of disorder and finiteness of the sample. Figures 7(a) and 7(b) show, respectively, the photonic band structure of s and p polarization thus ob-

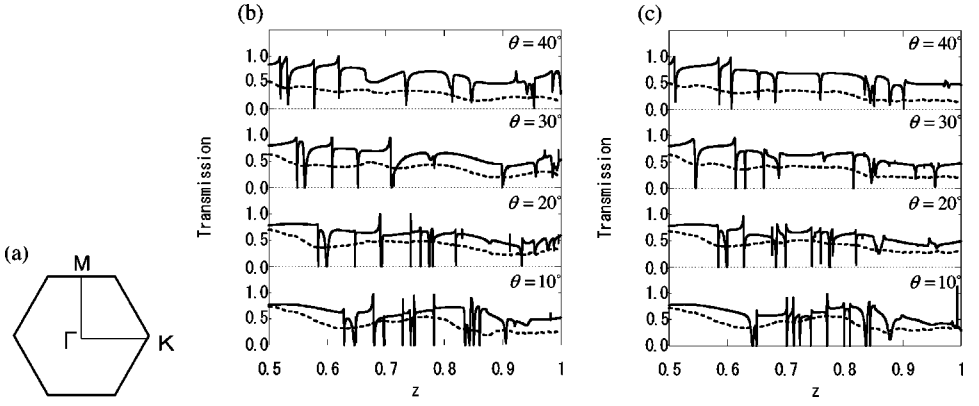

FIG. 6. (a) Brillouin zone of a triangular lattice. Transmission spectra for oblique incidence of p polarization. (b) For ΓK direction and (c) for ΓM direction. Incidence angles are chosen at 10°, 20°, 30° and 40°. Solid and dotted lines are theoretical and experimental results (Ref. 13), respectively.

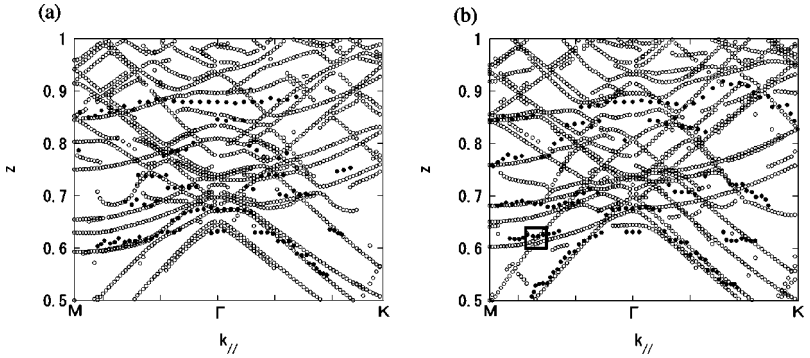

FIG. 7. Photonic band structures of (a) *s* and (b) *p* polarization. Band structures are obtained from transmission spectra by scanning the incidence angle θ. The horizontal and vertical axes represent in-plane wave vector and normalized frequency Z, respectively. Experimental results are shown by the filled circles and theoretical ones by the white circles. We will examine below in Fig. 9 the near-field intensity in the vicinity of the band crossing point encircled by the square in (b).

tained from transmission spectra by scanning θ. Experimental results are shown by filled circles and theoretical ones by white circles. One can see that bands for $Z \leqslant 0.7$ agree well with experimental results.

As can be seen, the band structure becomes very complicated due to the interaction between the monolayer and the substrate. However, we can qualitatively understand the origin of the band structure as follows. For this purpose, we give separately band dispersions of the monolayer and those of the substrate in Fig. 8. Filled circles in Fig. 8 show the band dispersion of the monolayer. Open circles and crosses in Fig. 8 show band dispersions of the substrate from Eqs. (13) and (14), respectively. Band dispersion of the substrate is obtained from the resonance condition of lights within the substrate from Eqs. (13) and (14) by changing $\mathbf{k}_{//}$ for fixed values of $\epsilon_S = 4.41$ and $d/a = 0.3$. The eigenstate of substrate is excited by diffracted light from the monolayer. Eigenstates of the substrate at $Z = 0.700$ and at $Z = 0.901$ at Γ point are six-fold degenerate. This degeneracy is lifted into three doubly degenerate states for ΓK direction, while they split into two single and two doubly degenerate states for ΓM direction. We can see that bands of the substrate and the monolayer overlap with each other to a large extent. Especially, bands in the range $0.6 \leqslant Z \leqslant 0.7$ for ΓM direction are considerably modified due to the interaction between the substrate and the monolayer.

While the overall feature of the band structure can be understood from the comparison between Figs. 7 and 8, it is difficult to identify the origin of branches at the band cross points. We have shown in the preceding section that near-field intensity gives valuable information for the classification of the origin of eigenstates at the Γ points. Below we use near-field intensity for oblique incidence to distinguish the difference of eigenstates. According to the preceding section, eigenstates of Γ point at $Z = 0.671$ and $Z = 0.808$ have different origin. Bands starting from these two states cross with each other in the vicinity of $Z = 0.61$ in the ΓM direction as is seen in the region encircled by the small square in Fig. 7(b). We examined near-field intensity in the vicinity of this cross point.

Figure 9(a) is the enlarged view near the cross point. The near-field intensity corresponding to the points P, Q, R, and S in Fig. 9(a) are shown in Fig. 9(Pu–Sℓ). Near-field intensity above the spheres and those at the upper plane of substrate are denoted by u and ℓ, respectively. Note that the shape of intensity distribution is rotated by 90° from Figs. 4(a) and 4(b) because the in-plane wave vector is along ΓM direction.

Figures 9(Pu) and 9(Pℓ) show near-field intensity at incident angle $\theta = 30°$ and $Z = 0.614$. Electric field is strongly enhanced near the substrate as in the case of Fig. 4(a). It turns out that this enhancement is due to the large y component of electric-field. In contrast, the z component is much smaller. These facts indicate that near-field intensity in Figs. 9(Pu) and 9(Pℓ) correspond to the eigenstates of the substrate of *s* polarization. Figures 9(Qu) and 9(Qℓ) show near-field intensity at $\theta = 30°$ and $Z = 0.630$. Two ellipses observed in Figs. 4(d) and 4(e) for perpendicular incidence merge into a

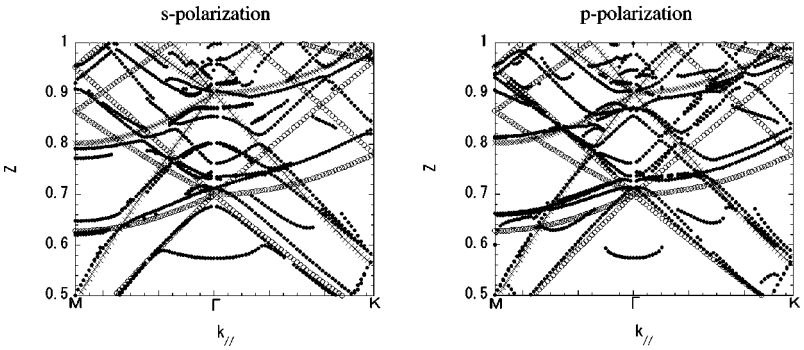

FIG. 8. Band dispersions of the monolayer spheres and those of the substrate. The horizontal and vertical axes are in-plane wave vector and normalized frequency Z, respectively. Filled circles show the band dispersion of the monolayer spheres. Open circles and crosses show the band dispersion of the substrate of *s* and *p* polarization, respectively.

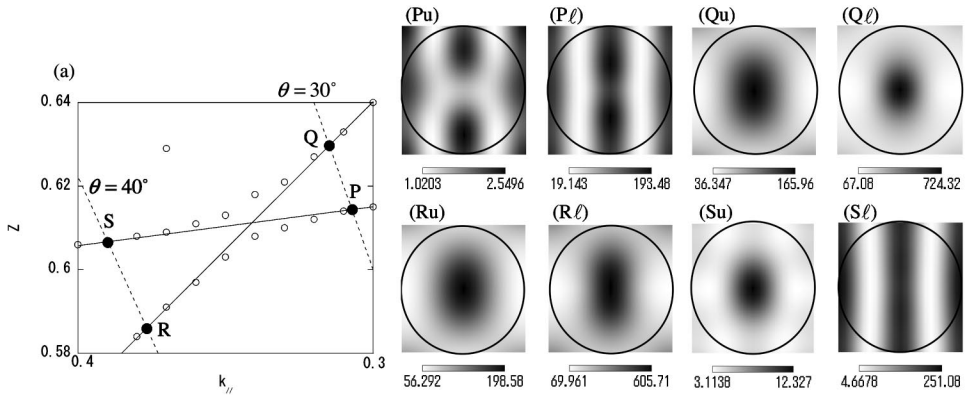

FIG. 9. (a) Enlarged view of the square region in Fig. 7(b). Bands of Fig. 7(b) are shown by white circles. Dotted lines are the in-plane wave vector component at incident angle $\theta=30°$ and $\theta=40°$. Each near-field intensity corresponds to points at $P:\theta=30°$; $Z=0.614$; $Q:\theta=30°$, $Z=0.630$; $R:\theta=40°$, $Z=0.586$; and $S:\theta=40°$, $Z=0.607$ in (a). Near-field intensity above the spheres and those at the upper plane of substrate at point *P*, for example, are respectively denoted as Pu and Pℓ.

single ellipse prolonged along the *y* axis. In this case, we observe the maximum field intensity of about 724 times larger than the incidence light. We also found large enhancement of the *z* component in the region between the monolayer and the substrate. This feature is common with that observed in Fig. 4(b). Figures 9(Ru) and 9(Rℓ) are near-field intensity at $\theta=40°$ and $Z=0.586$. These figures show a single ellipse like Figs. 9(Qu) and 9(Qℓ). There is thus a clear correspondence of near-field intensity between *Q* and *R*. This is also the case for *P* and *S* because the electric-field distribution and intensity of Fig. 9(Sℓ) at $\theta=40°$ and $Z=0.607$ are very similar to those of Fig. 9(Pℓ). Therefore, near-field intensity give fruitful information to figure out the origin of each eigenstate at the band cross point.

V. SUMMARY

We have numerically examined transmission spectra, band dispersions, and near-field intensity of the two-dimensional periodic dielectric spheres on the substrate of finite thickness. Transmission spectra for perpendicular incidence agree well with experimental results. We found that dips in transmission spectra for perpendicular incidence shift to lower frequencies due to the interaction with the substrate. It is also found that near-field intensity is much stronger than the system without the substrate. These effects are ascribed to the presence of eigenstates bounded within the substrate. Transmission spectra and band dispersions can be interpreted as a result of crossover phenomenon due to the interaction between eigenstates of the monolayer and those of the substrate. It is shown that near-field intensity can give detailed and fruitful information to investigate the origin of band eigenstates.

ACKNOWLEDGMENTS

The authors would like to thank K. Ohtaka, H. T. Miyazaki, S. Yamaguchi, and Y. Segawa for useful comments and valuable discussion. The authors are also grateful to H. T. Miyazaki for detailed information of the experimental results. This work was supported by a Grant-in-Aid for Scientific Research from the Ministry of Education, Science, and Culture.

*Email address: KUROKAWA.Yoichi@nims.go.jp

[1] J.D. Joannopoulos, R.D. Meade, and J.N. Winn, *Photonic Crystals* (Princeton University Press, Princeton, 1995); *Photonic Band Gaps and Localization*, edited by C.M. Soukoulis (Plenum, New York, 1993); *Photonic Band Gap Materials*, edited by C.M. Soukoulis (Kluwer, Dordrecht, 1996); P.M. Hui and Neil F. Johnson, in *Solid State Physics*, edited by H. Ehrenreich and F. Spaepen (Academic, New York, 1995), Vol. 49, p. 151.

[2] E. Yablonovitch, Phys. Rev. Lett. **58**, 2059 (1987).

[3] H. Kosaka, T. Kawashima, A. Tomita, M. Notomi, T. Tamamura, T. Sato, and S. Kawakami, Phys. Rev. B **58**, 10 096 (1998).

[4] S. Fan, P.R. Villeneuve, J.D. Joannopoulos, and E.F. Schubert, Phys. Rev. Lett. **78**, 3294 (1997).

[5] K. Ohtaka, Phys. Rev. B **19**, 5057 (1979).

[6] K. Ohtaka, J. Phys. C **13**, 667 (1980).

[7] K. Ohtaka and Y. Tanabe, J. Phys. Soc. Jpn. **65**, 2265 (1996).

[8] K. Ohtaka and Y. Tanabe, J. Phys. Soc. Jpn. **65**, 2670 (1996).

[9] K. Ohtaka and Y. Tanabe, J. Phys. Soc. Jpn. **65**, 2276 (1996).

[10] K. Ohtaka, T. Ueta, and Y. Tanabe, J. Phys. Soc. Jpn. **65**, 3068 (1996).

[11] T. Fujimura, T. Itoh, A. Imada, R. Shimada, T. Koda, N. Chiba, H. Muramatsu, H. Miyazaki, and K. Ohtaka, J. Lumin. **87-89**, 954 (2000).

[12] R. Shimada, Y. Komori, T. Koda, T. Fujimura, T. Itoh, and K. Ohtaka, Mol. Cryst. Liq. Cryst. Sci. Technol., Sect. A **349**, 5 (2000).

[13] H.T. Miyazaki, H. Miyazaki, K. Ohtaka, and T. Sato, J. Appl. Phys. **87**, 7152 (2000).

[14] T. Kondo, M. Hangyo, S. Yamaguchi, S. Yano, Y. Segawa, and K. Ohtaka, Phys. Rev. B **66**, 033111 (2002).

[15] G. Mie, Ann. Phys. (Leipzig) **25**, 377 (1908).
[16] M. Born and E. Wolf, *Principles of Optics* (Pergamon, Oxford, 1965), p. 633.
[17] M. Inoue, Phys. Rev. B **36**, 2852 (1987).
[18] N. Stefanou and A. Modinos, J. Phys.: Condens. Matter **3**, 8135 (1991).
[19] N. Stefanou and A. Modinos, J. Phys.: Condens. Matter **3**, 8149 (1991).
[20] G. Bosi, J. Opt. Soc. Am. B **13**, 1691 (1996).
[21] Y. Kurokawa, H. Miyazaki, and Y. Jimba, Phys. Rev. B **65**, 201102 (2002).
[22] H. Miyazaki and K. Ohtaka, Phys. Rev. B **58**, 6920 (1998).
[23] K. Ohtaka, H. Miyazaki, and T. Ueta, Mater. Sci. Eng., B **B48**, 153 (1997).
[24] K. Ohtaka, Y. Suda, S. Nagano, T. Ueta, A. Imada, T. Koda, J.S. Bae, K. Mizuno, S. Yano, and Y. Segawa, Phys. Rev. B **61**, 5267 (2000).